Supporting Information

A Multi-Modal Lateral Flow Assay Driven by MWCNTs/Fe-N-C for the Detection of Bisphenol A in Lake

Zhi-Ru Bi [b], *Ming-Hui Shi* [a], *Ting-Ting Chen* [b], *Yong-Biao Sun* [a], *Yu-Rui Zhou* [c], *Lin-Jing Wang* [a], *Huai-Rong Zhang* [a, *], *Guo-Dong Liu* [c, *].

a Collaborative Innovation Center of Tumor Marker Detection Technology, Equipment and Diagnosis Therapy Integration in Universities of Shandong, Shandong Province Key Laboratory of Detection Technology for Tumor Makers, College of Medicine, Linyi University, Linyi, 276005, China.

b Collaborative Innovation Center of Tumor Marker Detection Technology, Equipment and Diagnosis-Therapy Integration in Universities of Shandong, Shandong Province Key Laboratory of Detection Technology for Tumor Makers, School of Chemistry and Chemical Engineering, Linyi University, Linyi, 276005, China.

c Intelligent Biosensing Laboratory, College of Medicine, Linyi University, Linyi, 276005, China.

* Corresponding authors: zhanghuairong999@126.com; liuguodong2@lyu.edu.cn.

Experimental section

Material and reagents. Carboxylated multi-walled carbon nanotubes (MWCNT) with the length of >50 nm were purchased from Nanjing Xian-Feng Nanomaterials Technology Co., Ltd. carbodiimide hydrochloride (EDC), N-Hydroxysuccinimide (NHS), 3,3′,5,5′-tetramethylbenzidine (TMB), Pyrrole and Bisphenol A were obtained from Macklin Biochemical Co., Ltd (Shanghai). Streptavidin (SA), bovine serum albumin (BSA), and all the DNA oligonucleotides used herein were purchased from Sangon Biotechnical Engineering Co., Ltd. All the reagents were of analytical grade and solutions were prepared with ultrapure water.

The DNA oligonucleotide sequences were as follows:

Conjugated probe 1: 5'-NH_2C_6-ATCGACGGGTTCGCACCACCAGTG-3'.

T line probe: 5'-Bio-CCGGTGGGTGGTCAGGTGGGATAGCGTTCCGCGTAT GGCCCAGCGCATCACGGGTTCGCACCACACTGGTGGTGCGAACCCGTG-3'.

C line probe: 5'-bio-CACTGGTGGTGCGAACCCGTCGAT-3'.

Instruments. Transmission electron microscopy (TEM) images were carried out on JEM-F200 electron microscope (JEOL, Japan) and HT7800 (Hitachi, Japan). Zeta potential and size of nanoparticles were provided on zeta-sizer nano (Zen 3600, Malvern Instruments Ltd). The UV-vis absorption spectra recorded by UV-vis spectrophotometer (Cary60, Agilent). The functional group of nanoagents were performed by FT-IR spectrometer (Nicolet iS5, Thermo Scientific). The XYZ3010 dispensing platform and Guillotine cutting module CM3010 were purchased from Shanghai Jiening Biological Technology Co. Ltd. (Shanghai, China). The portable test

strip reader (DT2032) was bought from Shanghai Goldbio Tech. Co. Ltd. (Shanghai, China).

Transmission Electron Microscopy (TEM) Analysis. To observe the microstructural morphology of the materials, MWCNTs/Fe-N-C and MWCNTs/Fe-N-C/ssDNA$_1$ nanomaterials were individually dispersed in deionized water and subjected to ultrasonic treatment (40 kHz, 300 W, 15 min) to achieve a well-dispersed solution with nearly no color. A small amount of the dispersion was dropped onto a carbon-coated copper grid and air-dried. The samples were then examined using a transmission electron microscope (JEM-2100, Hitachi, Japan) to observe the morphological features, tubular structure, and surface coverage after ssDNA loading.

Zeta Potential and Particle Size Analysis. To evaluate the dispersibility and surface charge characteristics, MWCNTs/Fe-N-C and MWCNTs/Fe-N-C/ssDNA$_1$ nanomaterials were diluted to a nearly colorless dispersion and sonicated. The hydrodynamic particle size distribution and zeta potential were measured using a nanoparticle size and zeta potential analyzer (ZEN 3600, Malvern Instruments Ltd, UK). By comparing the particle size and zeta potential before and after ssDNA$_1$ loading, the surface modification efficiency and dispersion stability of the nanomaterials were further analyzed.

UV-Vis Absorption Spectroscopy Analysis. A UV-Vis spectrophotometer (UV-2600, Shimadzu, Japan) was used to record the absorption spectra of MWCNTs/Fe-N-C, MWCNTs/Fe-N-C/ssDNA$_1$, and free ssDNA$_1$. The samples were diluted and scanned over the wavelength range of 200-400 nm. Particular attention was paid to the

characteristic absorption peak at 260 nm to verify the successful immobilization of ssDNA$_1$ on the nanomaterial surface.

Peroxidase-like Activity and Steady-State Kinetic Assay of MWCNTs/Fe-N-C. The peroxidase-like catalytic activity of MWCNTs/Fe-N-C was evaluated using a TMB-H_2O_2 colorimetric system. Specifically, 20 μg/mL of MWCNTs/Fe-N-C was added to a PBS buffer solution (pH 5.8) containing 0.5 mM TMB and 10 mM H_2O_2. After incubation at room temperature (~ 25°C) for 10 minutes, the absorbance at 652 nm was recorded using a UV-Vis spectrophotometer to assess the formation of the blue-colored oxidized TMB (oxTMB) product.

To further investigate the catalytic kinetics, steady-state kinetic studies were performed by either fixing the TMB concentration at 500 μM and varying H_2O_2 concentrations (0.5, 1.0, 2.0, 3.0, 5.0, 10.0, 20.0, and 30.0 mM), or by fixing the H_2O_2 concentration at 10 mM and varying TMB concentrations (0.2, 0.4, 0.6, 0.8, 1.0, 1.2, 1.4, 1.6, and 1.8 mM). In each experiment, 20 μg of MWCNTs/Fe-N-C was dispersed in 1 mL PBS (pH 5.8), and the initial reaction rates were recorded.

The Michaelis-Menten plots were constructed based on the experimental data, and the kinetic parameters, including the Michaelis constant (K_m) and maximum reaction rate (V_{max}), were calculated using the Lineweaver-Burk double reciprocal plot, described by the following equation:

$$\frac{1}{\upsilon} = \frac{K_m}{V_{max} \times [S]} + \frac{1}{V_{max}} \quad \text{(Formula S1)}$$

Where υ is the initial reaction rate, [S] is the substrate concentration, K_m is the Michaelis constant, V_{max} is the maximum reaction rate.

$$\upsilon = \frac{c}{t} \quad \text{(Formula S2)}$$

$$A = \varepsilon \times l \times c \quad \text{(Formula S3)}$$

Where A is the absorbance value of the solution at 652 nm, ε is the molar extinction coefficient of oxTMB at 652 nm (3.9×10^4 M^{-1} cm^{-1}), l is the thickness of the solution, and c is the concentration of oxTMB.

This kinetic analysis provides insights into the substrate affinity and catalytic efficiency of MWCNTs/Fe-N-C.

Evaluation of Photothermal Capability of MWCNTs/Fe-N-C. To systematically evaluate the photothermal response performance of MWCNTs/Fe-N-C, 500 μL of a 50 μg/mL MWCNTs/Fe-N-C dispersion was placed in a transparent centrifuge tube. The sample was irradiated with an 808 nm near-infrared (NIR) laser at a power density of 2.0 W/cm² for 2 minutes. Temperature changes were recorded every 10 seconds using an infrared thermal imaging camera (FLIR E60, USA), and corresponding thermal images were captured to visually demonstrate the thermal response behavior of the material under NIR excitation. (Keep the spot size of 1 cm² and the irradiation distance of 5 cm unchanged.)

To further investigate the influence of material concentration and laser power on photothermal performance, dispersions of MWCNTs/Fe-N-C at concentrations of 12.5, 25, and 50 μg/mL were prepared and tested under the same irradiation conditions. Additionally, the laser power was adjusted to 0.5, 0.75, 1.0, and 1.25 W cm^{-2} to compare the temperature elevation profiles at different power levels, thereby revealing the relationship between concentration, laser power, and photothermal response.

To assess the photothermal stability of the material, five consecutive heating–cooling cycles were performed. For each cycle, the sample was irradiated for 2 minutes until the temperature reached its peak, followed by natural cooling to room temperature. This process was repeated five times, and the temperature rise and cooling curves of each cycle were recorded to evaluate the stability and repeatability of the material under repeated photothermal stimulation.

Based on the recorded temperature data, the photothermal conversion efficiency (η) was calculated using the Roper model equation as follows:

$$\eta = \frac{hS \cdot (T_{max} - T_{surr}) - Q_{dis}}{I(1 - 10^{-A808})} \quad \text{(Formula S4)}$$

Where hS is the heat transfer coefficient of the system, determined by fitting the cooling stage of the temperature curve; T_{max} and T_{surr} are the maximum and ambient temperatures, respectively; Q_{dis} represents the heat loss of the system, determined from control experiments without the material; I is the laser input power (W cm^{-2}); A808 is the absorbance of the material at 808 nm, obtained from UV-Vis spectroscopy measurements.

This analysis enables the quantification of the photothermal conversion efficiency of MWCNTs/Fe-N-C under different experimental conditions and provides fundamental data to support its application as a photothermal amplifier in multimodal detection platforms.

Aptamer Affinity Validation. The binding affinity between aptamers and bisphenol A (BPA) was verified via polyacrylamide gel electrophoresis (PAGE). Samples with

different components were loaded into the gel wells in a preset order, and the well distribution was detailed as follows:

Well 1: Molecular weight marker;

Well 2: Aptamer DNA_2 solution;

Well 3: Aptamer DNA_1 solution;

Well 4: Equal-volume mixture of DNA_2 and DNA_1;

Well 5: Incubated solution of DNA_2-DNA_1 mixture with BPA at a final concentration of 0.1 nM;

Well 6: Incubated solution of DNA_2-DNA_1 mixture with BPA at a final concentration of 1 nM;

Well 7: Incubated solution of DNA_2-DNA_1 mixture with BPA at a final concentration of 5 nM;

Well 8: Incubated solution of DNA_2-DNA_1 mixture with BPA at a final concentration of 10 nM;

Well 9: Incubated solution of DNA_2-DNA_1 mixture with BPA at a final concentration of 50 nM;

Well 10: Incubated solution of DNA_2-DNA_1 mixture with BPA at a final concentration of 100 nM.

All samples were loaded at a consistent volume of 6 μL. Prior to loading, the samples were denatured at 95 °C for 5 min and then placed on ice for 10 min to maintain the nucleic acid conformation.

The experimental results demonstrated that aptamers DNA_1 and DNA_2, either individually or in combination, maintained a stable nucleic acid conformation, with no significant non-specific binding observed between the two aptamers. Within the BPA concentration gradient of 0.1-100 nM, the binding of the aptamer mixture to BPA exhibited a distinct concentration dependence: low-concentration BPA (0.1 nM) could specifically bind to the aptamers, as evidenced by a significant reduction in the migration rate of gel bands; as the BPA concentration increased to 50-100 nM, the band migration rate reached a plateau, indicating that the binding between aptamers and BPA achieved a saturated state. In conclusion, the selected nucleic acid aptamers DNA_1 and DNA_2 in this study exhibited high affinity and specificity toward BPA, with a binding saturation concentration range of 50-100 nM. Moreover, effective binding was still achievable even at a low BPA concentration of 0.1 nM, which endows the aptamers with great potential for the detection of trace BPA in environmental samples.

Optimization of Multimodal Detection Performance. To achieve optimal colorimetric detection performance, several key parameters were systematically optimized, including the concentration of the T-line hairpin probe DNA_2, the amount of MWCNTs/Fe-N-C catalyst, the coupling concentration of $ssDNA_1$, and the spraying volume of the signal probe. A 100 μL standard sample solution was applied to the sample pad, and after incubation at room temperature for 30 minutes, the T-line signal intensity was measured using a portable strip reader to determine the optimal detection conditions.

For the catalytic colorimetric mode, further optimization was carried out by systematically evaluating the H_2O_2 concentrations (4, 6, 8, 10, and 15 mM) and their molar ratios with TMB. The optimal conditions were determined to achieve higher signal-to-noise ratios and lower detection limits, ensuring the efficient detection of BPA.

Specificity Analysis. To validate the molecular recognition specificity of the platform for BPA, structurally similar compounds, including bisphenol S (BPS), bisphenol F (BPF), phenol, and nonylphenol (NP), were used as interference controls. The signal responses were evaluated under three detection modes: colorimetric, catalytic colorimetric, and photothermal. By comparing the T-line signal intensities of different analytes, the platform's high specificity for BPA was confirmed, effectively avoiding false-positive signals from interfering substances and ensuring the accuracy and reliability of the detection results.

Real Sample Analysis and Recovery Evaluation. To assess the applicability of the LFA platform for detecting BPA in real environmental samples, lake water samples were collected, filtered through 0.22 μm membranes to remove impurities, and then appropriately diluted. The lake water sample was collected from Binhai Lake of Linyi University. Its key water quality parameters are as follows: pH 7.63, conductivity 112.86 μS/cm, dissolved oxygen 10.23 mg/L, dissolved organic carbon (DOC) 5.84 mg/L, total nitrogen (TN) 1.98 mg/L, and total dissolved solids 126 mg/L. The concentrations of major inorganic ions in the water are within the normal range of natural freshwater lakes. The water sample has low background impurity content and

191 weak overall matrix interference. Known concentrations of BPA (0.5, 5, and 50 ng/mL)
192 were spiked into these samples for recovery experiments. Detection was carried out
193 following the optimized procedures, and the recovery was calculated using the
194 following equation:

195 $$\text{Recovery} = \frac{\text{Measured Concentration}}{\text{Spiked Concentration}} \times 100\% \quad \text{(Formula S5)}$$

196 In addition, the relative standard deviation (RSD) was calculated to evaluate the
197 repeatability and stability of the detection. By comparing the recovery rates and RSD
198 values at different spiking concentrations, the accuracy and reliability of the multimodal
199 LFA platform for detecting BPA in real water samples were comprehensively validated.
200

Supporting Figures

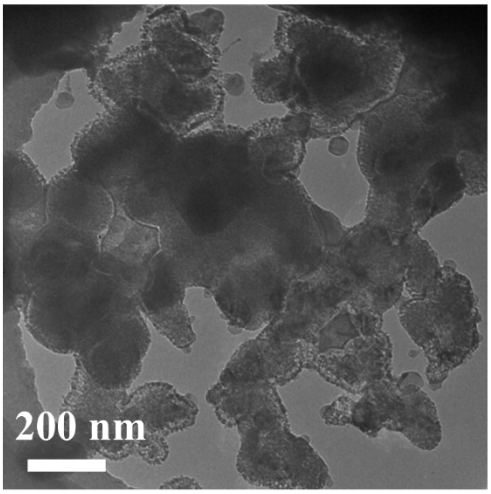

Figure S1 TEM image of MWCNTs/Fe-N-C/ssDNA$_1$.

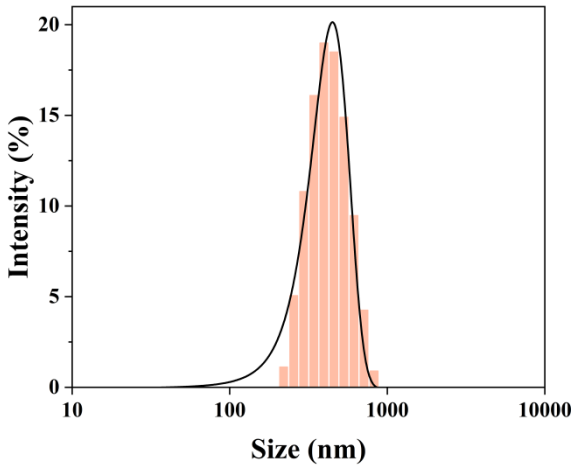

Figure S2 Hydrodynamic size distribution of MWCNTs/Fe-N-C/ssDNA$_1$.

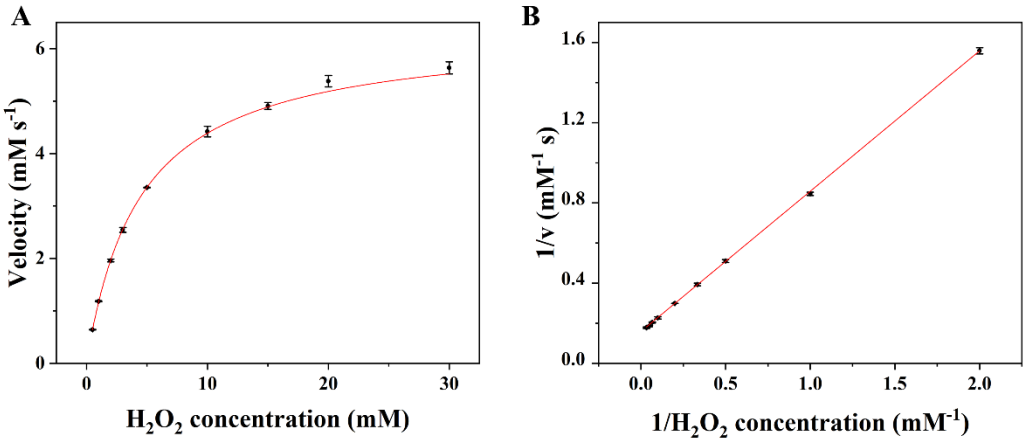

Figure S3 A) Michaelis-Menten curve of MWCNTs/Fe-N-C and B) Lineweaver-Burk (L-B) plot derived from the kinetic data with H_2O_2 as the substrate.

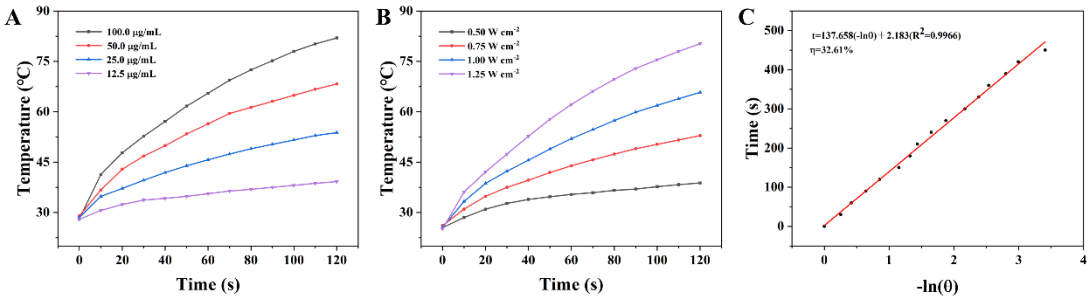

Figure S4 A) Photothermal heating curves of MWCNTs/Fe-N-C dispersions with different concentrations under 808 nm laser irradiation. B) Temperature elevation of MWCNTs/Fe-N-C dispersions under different laser power densities. C) Comparison of photothermal conversion efficiencies before and after $ssDNA_1$ modification on MWCNTs/Fe-N-C.

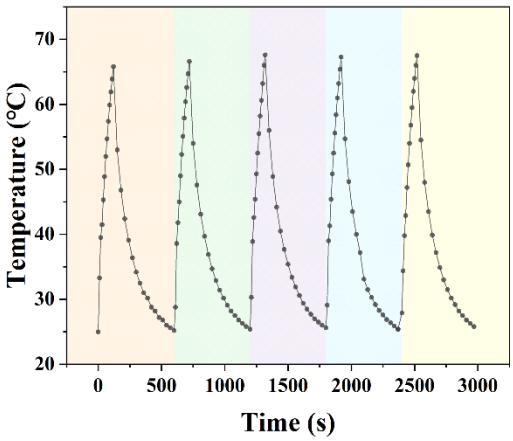

221

222 Figure S5 Photothermal stability of MWCNTs/Fe-N-C/ssDNA$_1$ evaluated by five

223 consecutive heating-cooling cycles.

224

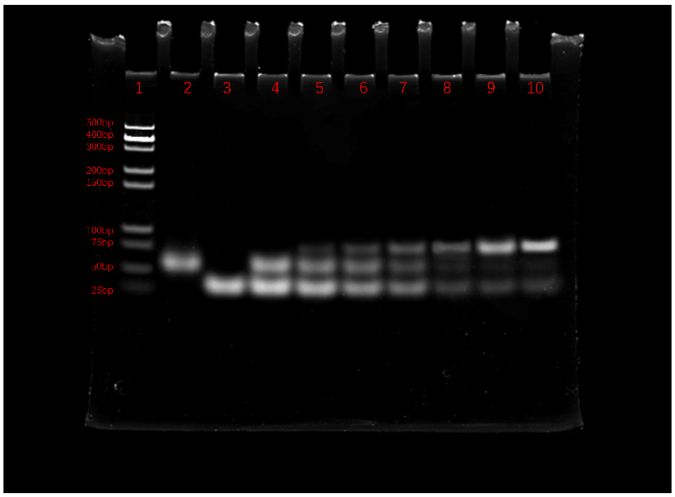

225

226 Figure S6 Polyacrylamide Gel Electrophoresis (PAGE) Image.

227

228

229 Figure S7 Heat map of the recoveries of developed multimodal LFA for the detection

230 of BPA in lake samples.

Table S1. Comparison of related studies reported in the past three years.

Method	Material	Year	LOD	Linear range
This work	MWCNTs/Fe-N-C	2026	0.047 ng/mL	0.05-1000 ng/mL
Test strip	AuNPs	Komova *et al.* (2024)	13.5 ng/mL	0.05-0.25 μg/mL
Test strip	MPs/QDs	Aranova *et al.* (2025)	0.03 μg/mL	0.3-100 μg/mL
Electrochemical sensor	Ag@NC/PEI	Shim *et al.* (2026)	1.43 ng/mL	22-2200000 ng/mL
HPLC	pH-responsive DES	Cao & Li (2024)	0.05ng/mL	0.1-50 ng/mL

[1] N. S. Komova, K. V. Serebrennikova, A. N. Berlina, A. V. Zherdev and B. B. Dzantiev, *Journal of Analytical Chemistry*, 2024, 79, 476-485.
[2] N. A. Taranova, A. A. Bulanaya, A. V. Zherdev, B. B. Dzantiev, *Sensors*, 2025, 25, 7328.
[3] K. Shim, M. M. Karim, S. Park, H. K. Lee, D. Lee, J.-S. Bae, D.-S. Park, H. J. Kim, *Applied Surface Science*, 2026, 731, 166391.
[4] L. Cao and Y. Li, *Journal of Separation Science*, 2024, 47, e2300776.